Charge of a quasiparticle in a superconductor

Yuval Ronen[†1], *Yonatan Cohen*[†1], *Jung-Hyun Kang*[1], *Arbel Haim*[1], *Maria-Theresa Rieder*[1,2], *Moty Heiblum*[#1], *Diana Mahalu*[1] *and Hadas Shtrikman*[1]

[1]*Braun Center for Submicron Research, Department of Condensed Matter Physics, Weizmann Institute of Science, Rehovot* 76100, *Israel*

[2]*Dahlem Center for Complex Quantum Systems, Freie University, Berlin* 14195, *Germany*

[†] *Equal contributions*

[#]*Corresponding Author* (*moty.heiblum@weizmann.ac.il*)

Methods and Supplementary Information

In this Supplementary Section we add details that could not find room in the main text. We placed a brief review of the theoretical background as well as the simulation. In addition, a few details of the NWs growth process followed by the fabrication process are provided, as well as more details on the conductance and noise measurements.

S1 – Theoretical model

Scattering theory of multiple Andreev reflections

Following [1, 2], we here outline the calculation of the current and current noise through a SNS-Josephson junction in the formalism of multiple Andreev reflections. Where electrons in the normal part are Andreev reflected from the superconducting leads. The normal region contains a barrier whose transmission amplitude squared is t. It is assumed that the length of the normal region is much smaller than the superconducting coherence length, and that the Fermi energy in the normal region is much larger than the superconducting gap Δ. As a simplified setup we consider a short one-dimensional normal metal piece connected to one-dimensional semi-infinite superconducting leads.

A voltage biased Josephson junction exhibits a phase divergence that increases linearly in time as $\varphi(t)=2eVt/\hbar$. This poses a periodically time-dependent problem which may be treated using Floquet theory expanding the eigenstates of the system in the quasi-energies $\varepsilon+2neV$. A physical interpretation of these energies is in general not straightforward. However, in our specific case they are just the energies of the electrons/holes in the junction after multiple Andreev reflections. For instance, consider a voltage bias $eV<<\Delta$ and an electron injected into the junction at energy $\varepsilon\le-\Delta$ from the left lead- in equilibrium with a chemical potential μ. After propagating through the junction this electron is Andreev reflected around the equilibrium potential of the right lead, $\mu-eV$, and returns as a hole with an energy $-\varepsilon-2eV$. Here, it is again Andreev reflected into an electron with energy $\varepsilon+2eV$. This process repeats until the particle has gained enough energy to overcome the superconducting gap and can be absorbed into the continuum of quasi-particle excitations in one of the leads.

Following the picture of multiple Andreev reflections, we can set up the wave-functions of the electronic state in the junction at the boundaries to the two leads, X_1, X_2 respectively. With the quasi-energies measured with respect to the chemical potential of the left lead, the wave-function for a quasi-particle incident on the junction from the left lead is

$$\phi(x_1,t)=\frac{J(\varepsilon)}{\sqrt{2\pi v_F}}\sum_{n=-\infty}^{\infty}\left[\begin{pmatrix}a_{2n}A_n+\delta_{n,0}\\A_n\end{pmatrix}e^{ikx_1}+\begin{pmatrix}B_n\\a_{2n}B_n\end{pmatrix}e^{-ikx_1}\right]\cdot e^{-i(\varepsilon+2neV)t}$$

$$\phi(x_2,t)=\frac{J(\varepsilon)}{\sqrt{2\pi v_F}}\sum_{n=-\infty}^{\infty}\left[\begin{pmatrix}C_n\\a_{2n+1}C_n\end{pmatrix}e^{ikx_2}+\begin{pmatrix}a_{2n+1}D_n\\D_n\end{pmatrix}e^{-ikx_2}\right]\cdot e^{-i(\varepsilon+2neV)t}$$

Where we chose a spinor in the basis $\left(c_\uparrow,c_\downarrow^\dagger\right)$ normalized to flux. The quasi-particle enters the junctions as an electron with probability $J(\varepsilon)=\sqrt{1-|a(\varepsilon)|^2}$, with the Andreev reflection amplitude $a(\varepsilon)=\left(\varepsilon-i\sqrt{\Delta^2-\varepsilon^2}\right)/\Delta$ if $\varepsilon\le\Delta$ and $a(\varepsilon)=\left(\varepsilon-sgn(\varepsilon)\sqrt{\Delta^2-\varepsilon^2}\right)/\Delta$ if $\varepsilon\ge\Delta$.

The tunneling barrier in the normal part of the junction with transmission $t \le 1$ is implemented by a scattering matrix connecting the amplitudes of the left and the right side in a recursive fashion

$$\begin{pmatrix} B_n \\ C_n \end{pmatrix} = S \begin{pmatrix} a_{2n} A_n + \delta_{n,0} \\ a_{2n+1} D_n \end{pmatrix} \quad \text{and} \quad \begin{pmatrix} A_n \\ D_{n-1} \end{pmatrix} = S^* \begin{pmatrix} a_{2n} B_n \\ a_{2n-1} C_n \end{pmatrix}$$

$$S = \begin{pmatrix} r & d \\ d & -r^* d / d^* \end{pmatrix}$$

with $|d|^2 = t$.

The current $\hat{I}(t) = \frac{-ie\hbar}{2m} \sum_\sigma \left(\psi_\sigma^\dagger(t) \partial_x \psi_\sigma(t) - h.c. \right)$ may be evaluated at, say, the left boundary using the fact that each lead individually is in equilibrium. The electronic states are constructed from the Bogoliubov quasiparticle operators $\hat{\gamma}$ in the superconducting lead as $\psi_\sigma(t) = \sum_\nu \left(u_\nu(t) \hat{\gamma}_{\sigma,\nu} + sgn_\sigma \, u_\nu^*(t) \hat{\gamma}_{-\sigma,\nu} \right)$. We are using a joint index $\nu = i, \varepsilon$ to indicate the origin and energy of the incident electron ($i = l, r$ for the left and right lead). The wave-function $u_\nu(t) / \upsilon_\nu(t)$ is the respective electron/hole amplitudes obtained from solving the recursive relations denoted above. Our main interest in this work is the low-frequency current-noise, which is given by the zero Fourier component of the time averaged, symmetrized current correlation:

$$S(V) = \int d\tau \overline{\left\langle \delta\hat{I}(t) \delta\hat{I}(t+\tau) + \delta\hat{I}(t+\tau) \delta\hat{I}(t) \right\rangle}$$

where $\delta\hat{I}(t) = \hat{I}(t) - \left\langle \hat{I}(t) \right\rangle$, and the upper bar stands for time averaging (see [1, 2] for the explicit expressions). To comply with the experimentally measured quantity $S_{\text{exc}}(V)$, one subtracts from $S(V)$ the noise at zero voltage $S(V \to 0)$. For the experimentally-relevant temperatures and voltages this contribution is negligible.

Details on the numerical calculations

The solution to the recurrence relations described above is found using the method of continued fractions, following [3, 4]. First, the amplitudes A_n, C_n, D_n are eliminated yielding a recursive equation for the B_n of the general form

$$c_n B_{n+1} - d_n B_n + c_{n-1} B_{n-1} = -\delta_{n0}$$

Introducing a new variable $X_n = \frac{B_n}{B_{n-1}}$ for $n > 0$ and $X_n = \frac{B_n}{B_{n+1}}$ for $n < 0$, for a sufficiently large $n_{\max} >> 2\Delta / eV$. The physical reasoning of this ansatz is that an electron impinging a lead above the gap is absorbed with a probability approaching 1 rapidly for high energies. Hence, the amplitudes of states in the junction at high enough energies - corresponding to $n > n_{max}$ - are negligible. Following this procedure one can find all coefficients B_n except for B_0, which is then obtained directly from Eq. (5) as

$$B_0 = \left(c_0 X_1 - d_0 + c_{-1} X_{-1} \right)^{-1}$$

Additional simulations

Noise in a NIS junction:

We here calculate the current and current noise in a junction of a normal metal (N) and a superconductor (S) with a tunneling barrier in the middle to model the insulating region (see Fig. S1). Transport through this kind of systems has been studied abundantly in the literature and we here adapt the formalism of Refs. [5, 6] to calculate the noise using the scattering matrix, particularly the reflection matrix with electron-hole grading

$$r(\varepsilon) = \begin{pmatrix} r_{ee}(\varepsilon) & r_{eh}(\varepsilon) \\ r_{he}(\varepsilon) & r_{hh}(\varepsilon) \end{pmatrix}$$

of excitations at energy ε (of either an electron or a hole) approaching the junction from the normal metal. The tunneling barrier is described by a normal scattering matrix for electrons

$$S_I = \begin{pmatrix} \rho & \tau \\ \tau & \rho' \end{pmatrix}$$

with the transmission $|\tau|^2 = t$ and $\rho' = -\rho^*\tau/\tau^*$ assumed to be energy independent, and the corresponding matrix for holes is then just S_I^*. The N-S interface is described by the Andreev-reflection amplitude $a(\varepsilon)$ given by

$$a(\varepsilon) = \frac{1}{\Delta}\begin{cases} \varepsilon - sgn(\varepsilon)\sqrt{\varepsilon^2 - \Delta^2} & ,|\varepsilon| > \Delta \\ \varepsilon - i\sqrt{\Delta^2 - \varepsilon^2} & ,|\varepsilon| < \Delta \end{cases}.$$

The reflection amplitudes $r_{ee}(\varepsilon)$ and $r_{he}(\varepsilon)$ are found from an infinite series expansion considering all possible paths through which an incident electron is reflected as an electron or as a hole respectively. Taking the distance between the normal barrier and the S-N interface to zero, one obtains

$$r_{ee}(\varepsilon) = \rho + \tau a(\varepsilon)\rho'^* a(\varepsilon)\tau + \tau a(\varepsilon)\rho'^* a(\varepsilon)\rho' a(\varepsilon)\rho'^* a(\varepsilon)\tau + \ldots = \rho + \frac{\tau^2\rho'^* a^2(\varepsilon)}{1 - |\rho|^2 a^2(\varepsilon)}$$

$$r_{he}(\varepsilon) = \tau a(\varepsilon)\tau^* + \tau a(\varepsilon)\rho'^* a(\varepsilon)\rho' a(\varepsilon)\tau^* + \ldots = \frac{|\tau|^2 a(\varepsilon)}{1 - |\rho|^2 a^2(\varepsilon)}$$

Defining $R_{ee}(\varepsilon) = |r_{ee}(\varepsilon)|^2$ and $R_{he}(\varepsilon) = |r_{he}(\varepsilon)|^2$, the current and current noise at zero temperature are then obtained by [2]

$$I = \frac{2e^2}{h}\int_0^{eV} d\varepsilon\left[1 - R_{ee}(\varepsilon) + R_{he}(\varepsilon)\right]$$

$$S = \frac{4e^2}{h}\int_0^{eV} d\varepsilon\left[R_{ee}(\varepsilon)\left[1 - R_{ee}(\varepsilon)\right] + R_{he}(\varepsilon)\left[1 - R_{he}(\varepsilon)\right] + 2R_{ee}(\varepsilon)R_{he}(\varepsilon)\right]$$

We calculated the ratio $S/2eI$ which does not show a dip around $eV=\Delta$ even though the current shows a peak from enhanced tunneling into the superconductor due to a singularity in the density of states.

S2 - MBE Growth and sample fabrication

MBE Growth of InAs NWs. The high-quality InAs NWs used in this study were grown by the Au-assisted, vapor-liquid-solid (VLS) method, in a high purity molecular beam epitaxy (MBE) system [7]. The epi-ready (111)B InAs substrate, glued onto a lapped silicon (Si) wafer, was initially heated in an 'introduction chamber' to 180^{O}C for water desorption, followed by degassing at 350^{O}C and a subsequent oxide blow-off with no intentional arsenic overpressure (in a dedicated treatment chamber attached to the MBE system). A thin layer of Au (less than 1*nm* thick) was subsequently evaporated in the same chamber. Following transfer to the growth chamber, the substrate temperature was ramped up to ~550^{O}C for ripening the Au layer into droplets with a rather uniform size and density distribution [7]. Lowering the growth temperature (to ~400^{O}C), InAs growth was initiated with an As_4/In flux ratio of ~100, with resultant InAs NWs nucleating at the Au droplets and growing to a length of ~4-5μ*m* with a diameter of 50-60*nm*. The NWs grow along the <0001> direction and have a pure Wurtzite structure mostly without any stacking faults (as verified by TEM imaging).

Device fabrication. The sample was fabricated on a thermally oxidized Si/SiO_2 substrate ($Si:p^+$ doped and acts as a back gate). The NWs were detached from the growth surface by sonication, in ethanol and a droplet, later to dry, placed on a substrate with pre-arranged optical marks. Native oxide was removed and surface passivated with an ammonium polysulphide solution $(NH_4)_2S_x$=1:5, with the NWs immediately transferred into an evaporation chamber. Superconducting contacts, 5/120nm Ti/Al thick, were evaporated by electron beam evaporation.

S3 – Detailed measurement setup

Figure S3 provides a detailed schematic diagram of the measurement setup. The experiment was performed in a dilution refrigerator, with an electron temperature of ~25mK, (inside the dashed region). The Josephson junction is voltage biased (with 5Ohms resistance at the Source), allowing access of all quiescent points in the *I-V* characteristic. Two electrical relays were employed, one at the input (at 300K) and one at the output (at 25mK); allowing switching from low frequency measurement (mode 1) - using the lock in technic, to a higher frequency (mode 2) - using a function generator and a spectrum analyzer. The actual measurements were done in mode 2, while measurements in mode 1 were performed in order to calibrate the higher frequency measurement.

Mode 1 – *low frequency measurement*

A calibration line allows calibrating the 5Ohms resistor after cooling. Applying DC voltage plus an AC signal and measuring the two-terminal AC current, allows calculating the static and dynamic conductance. The current was amplified by an external current amplifier [8], with 10^7V/A conversion factor, followed by a DMM or a lock-in amplifier. The measured differential conductance was used to calibrate the higher frequency measurements.

Mode 2 – *higher frequency measurement*

While at DC the Drain is shorted through the coil *L*, the 600 kHz signal is divided between the junction resistance and R_L. The external voltage amplifier, SA-220F5, has a gain of 200, while the home-made 'cold' voltage preamplifier has a gain ~5. Noise measurements were performed by replacing the function generator (needed for the conductance measurements) with a DC source, and increasing the bandwidth of the spectrum analyzer. In our setup we also have two kinds of low pass filters, LPF_1 and LPF_2 which differ by their cut-off frequency. LPF_1 is placed both in RT and in base-temperature has a cutoff frequency of 80MHz (mini-circuit BHP-100+). LPF_2 is placed between them, also in base temperature and has a cut-off frequency of 2MHz.

S4 - Estimating the background noise

The total voltage noise per unit frequency at the input of the 'cold' preamplifier:

$$S = S_{exc} r^2 + i_{amp}^2 r^2 + \upsilon_{amp}^2 + 4k_B T r \qquad \left[V^2 / Hz \right], \quad \text{(S1)}$$

where S_{exc} is the excess current noise per unit frequency, i_{amp} and υ_{amp} are the amplifier's current and voltage noises, respectively, T is the temperature and r is the resistance that the amplifier 'sees' at the resonance frequency (with a small frequency window):

$$r = R_{sample} \| R_L = \frac{R_{sample} R_L}{R_{sample} + R_L} \quad ,$$

here R_{sample} is the differential resistance of the sample and R_L is the frequency independent load resistance. Note, that the $1/f$ contribution to the noise at f_0=600kHz is negligible. This is justified both from our measurements at high magnetic field as explained in S6 as well as from previous noise measurements done in our system to accurately extract integer and fractional charges of excitations in various 2DEG systems.

The background noise, subtracted from the total noise, is:

$$S_{BG} = i_{amp}^2 r^2 + \upsilon_{amp}^2 + 4k_B T r \qquad \left[V^2 / Hz \right]. \quad \text{(S2)}$$

Since the differential resistance is strongly dependent on biasing voltage V_{SD}, we first describe the procedure of determining the background noise. Since this noise (measured at zero bias) is laden with an emerging large Josephson current, it is quenched by applying a magnetic field stronger than B_c (B~200mT), where the superconductivity is quenched. The differential conductance and the background noise were then measured as a function of the back-gate voltage, and thus as function of r, in the relevant range (Fig. S4). The values of the amplifier's noises obtained by fitting are in good agreements with the values we measure using other calibration methods. The electron temperature agrees well with that measured by other shot noise measurements.

S5 – The critical magnetic field

In order to find the critical magnetic field, MAR conductance peaks are measured as a function of the magnetic field, with the spacing between the peaks directly proportional to the diminishing superconducting gap with magnetic field (Fig. S5).

S6 – Number of conducting channels in the bare NW

Under high enough magnetic field the quantum charge passing the junction is that of the electron. The expression for shot noise provided in the text is that of a singly occupied spin-degenerate conducting channel,

$$S_{exc} = 2eI(1-t) \quad \text{and} \quad t = \frac{G}{g_Q} \quad , \qquad \text{(S3)}$$

where G is the conductance and g_Q is the quantum of conductance $g_Q = 2\frac{e^2}{h}$.

The differential conductance and the I-V_{SD} characteristic were measured after quenching superconductivity (but not lifting spin degeneracy) at the working voltage of the back-gate corresponding to the actual experiment (Figs. S6a and S6b). The noise is then measured as a function of V_{SD} (blue curve in Fig. S6c), and the background noise is subtracted (red curve in Fig. S6c), and the excess noise is plotted in Fig. S6d. The theoretical curve, calculated using Eq. S4, plotted in a black dashed line, seems to agree nicely with the data. In order to test this further, we also plot the expected excess noise assuming two spin-degenerate channels, namely,

$$S_{exc} = 2eI_1(1-t_1) + 2eI_2(1-t_2) \qquad \text{(S4)}$$

With I_1 and I_2 the current carried by each of the two channels, while t_1 and t_2 are the transmission of each of the two channels. If the total current, I, splits between the two channels in the following way

$$I_1 = \alpha I \qquad I_2 = (1-\alpha)I \quad , \qquad \text{(S5)}$$

then,

$$t_1 = \alpha\frac{G}{g_Q} \qquad t_2 = (1-\alpha)\frac{G}{g_Q} \quad . \qquad \text{(S6)}$$

Therefore, since we know *I* and *G*, we can plot S_{exc} for a given α. In Fig. S6d we plot S_{exc} for α=0.5 0.4 0.3 0.2 0.1 and 0.0. Note that α=0, being the single channel case, indeed fit best the data.

This measurement also allows us to show that the 1/f noise to the total noise is negligible. Since the 1/f noise is proportional to I^2, any non-negligible contribution of it would cause noise dependency on the current to deviate from formula S4 and to become non-linear. Since our measurement in Fig 6d is linear and completely coincides with the above formula we conclude that the 1/f noise is negligible.

S7 – Nature of tunneling quasiparticles

Three possible models are suggested to account for the single quasiparticle tunneling taking place in the junction. We calculated the Fano-factor (*F*) for the models in order to see which one of them can account for the measured charge at the superconducting gap's edge – being smaller than *e* at a low transmission. In each table, we express the probability of an event to take place P(x) and its charge (X):

Model 1: Quasiparticles of charge *e* tunneling with probability *t*.

x	P(x)
0	*(1-t)*
e	*t*

$$\mu = et$$
$$\sigma^2 = e^2 t(1-t)$$
$$F = \frac{\sigma^2}{\mu} = e(1-t) \xrightarrow{t \to 1} e$$

Model 2: Quasiparticles of charge *e** tunneling with probability *t* and collapse as an electron with a probability *p* or as a hole with probability *q*, with *p*+*q*=1.

x	P(x)
0	*1-t*
e	*tp*
-e	*tq*

$$\mu = et(p-q)$$
$$\sigma^2 = e^2 t - e^2 t^2 (p-q)^2$$
$$F = \frac{\sigma^2}{\mu} = e\frac{1-t(p-q)^2}{(p-q)} \xrightarrow{t \to 1} e\frac{1}{(p-q)} > 1$$

Model 3: Quasiparticles of charge e^* tunneling as a composite particle with probability t.

x	P(x)
0	*(1-t)*
e^*	t

$$\mu = e^* t$$
$$\sigma^2 = e^{*2} t(1-t)$$
$$F = \frac{\sigma^2}{\mu} = e^*(1-t) \xrightarrow{t \to 1} e^*$$

It is important to mention that the models above are considering only single quasiparticle tunneling across the junction neglecting higher order MAR contributions. When we lower the transmission we suppress the higher order MAR contributions and reveal a dip in the charge. This is clearly seen in our data as well as in the results of the theoretical model of **S1**. Once we suppressed these high order MAR contributions we observe a Fano factor which is smaller than e, which is only consistent with Model 3 above. In other words, the only way to observe a Fano factor that is lower than e is both to suppress enough the high order MAR (going to low transmissions) as well as having a tunneling of quasiparticles carrying a fractional charge.

S8 – Induced superconductivity on a single band

In this section we aim to support our claim in the manuscript for having a non-BCS density of state and specifically a sharper one in our 1D system.

Observing figure 3a in the main text it is possible to see negative differential conductance, this effect which is more apparent as the transmission is decreased originates as we will show from the change in the usual BCS density of states.
In figure S7 (a&b) we plot a measurement of the differential conductance as a function of the applied bias and the I-V curve. In figure S7 (c&d) we plot the theoretical predicted I-V curve and differential conductance based on the BCS density of state assuming a uniform transmission. The negative differential resistance which is clearly seen in the measurement and manifested in the experimental I-V curve as a peak in the current is not visible in the theoretical I-V, this suggests a different theoretical model should be given.

The origin of this discrepancy is the assumption of a linear dispersion which usually one considers in calculating the DOS. In a 1D wire, which has a parabolic dispersion, as the Fermi level is lowered to the bottom of the conduction band this assumption

fails. Hence, the change in the DOS is more apparent as the fermi energy gets closer to the 'Van-Hove singularity'.

To show this we calculated the DOS and I-V curves as a function the fermi energy position. Figure 8(a, d and g) are the density of state for E_F=5Δ, 2Δ and Δ respectively. In figure 8(b, e and h) we plot each DOS when the fermi energy is defined as zero energy. It is already clear that as the Fermi level is pushed towards the bottom of the band the DOS is modified. In Fig 8(c, f and i) we calculate the I-V curves and show that the modified DOS gives rise to a peak in the I-V curve, similar to the one we showed in fig S7b.
In conclusion, the negative differential resistance which is seen in experiment as the device is pinched suggests a modification from the usual BCS density of state.

S9 – Charge partition in SIN junction

In the SIS junction, the overlap between filled states of quasiparticles' wave-function and empty states (above the gap) in the two superconductors allows **tunneling** of quasiparticles with fractional charge. However, in the case of SIN, in the N side there are quasiparticles with charge ***e*** while in the S side there are quasiparticles with a **smaller charge**. Our physical picture suggests that tunneling of electrons, being of the higher charge is always dominant. In one polarity, the electrons that tunnel from N to S breaks to multiple quasiparticles; while in the opposite polarity, quasiparticles bunching to an electron (in N) takes place. This is similar to the known bunching in the $\nu = 1/3$ fractional quantum hall states where 3 quasiparticles, each with charge *e*/3, tunnel together to form an electron.

Moreover, and in general, tunneling between two different materials, with different quasiparticles in each side, the current fluctuations will correspond to the larger charge transfer. For example, when the bias is smaller than Δ, electrons from the N region "bunch" to form Cooper pairs and the measured charge (via shot noise) is **2*e*** (via Andreev reflection).

References

[1] D. Averin and A. Bardas, Phys. Rev. Lett. **75**, 1831 (1995).

[2] Y. Naveh and D.V. Averin, Phys. Rev. Lett. **82**, 4090 (1999).

[3] E.N. Bratus and V.S. Shumeiko, Sov. Phys. Solid State. **21**, 1506 (1979).

[4] E.N. Bratus, V.S. Shumeiko and G. Wendin, Phys. Rev. Lett. **74**, 2110 (1995).

[5] C. W. J. Beenakker, Rev. Mod. Phys. **69**, 731 (1997)

[6] M. P. Anantram and S. Datta, Phys. Rev. B **53**, 16390 (1996)

[7] IEEE J. of Selected Topics in Quantum Electronics, (2011), 17(4) 922-934.

[8] A. V. Kretinin, Y. Chung, wide-band current preamplifier for conductance measurments with large input capacitance, Rev. Sci, Instrum. 83, 084704 (2012)

Figure Captions:

Figure S1. The Junction is modeled by a combination of a normal barrier and a perfect N-S interface. The calculation is done in the limit where the distance between the barrier and the N-S interface is zero.

Figure S2. SEM image of InAs NWs grown on (111)B InAs (micrograph taken at 45º). Note the uniformity of width and length of the NWs.

Figure S3. Measurement setup. A scanning electron micrograph of the device (scale bar, 200nm) connected to a detailed illustrated circuit.

Figure S4. Background noise measurements. (a) We start by measuring the differential conductance, G_{sample}, as a function of back gate voltage, V_g. The differential resistance is given by $R_{\text{sample}}=1/G_{\text{sample}}$ and is shown in (b). Then we calculate the resistance that the amplifier sees at its input, R_{parallel}, by taking R_{sample} in parallel to R_L and the result is shown in (c). (d) We then measure the background noise as a function of back gate voltage, V_g. This is done at magnetic field of 200mT to avoid effects related to superconductivity, and at zero bias to avoid any Shot noise. Combining the results allows us to plot the background noise as a function of G_{sample} as shown in (e), or as a function of R_{parallel} as shown in (f). In (f) we show the fit of the final result to a second order polynomial from which we obtain the coefficients of Eq. S2.

Figure S5. **Critical magnetic field of the Al contacts.** Differential conductance as a function of bias and magnetic field.

Figure S6. **Noise measurements at high magnetic field.** (a) Differential conductance vs. bias, V_{SD}, at magnetic field of 200mT. (b) *I-V* curve obtained by integrating the differential conductance. (c) Total voltage noise (in blue) and background noise (red) as a function of bias. (d) Excess current noise per unit frequency as s function of DC current through the device is plotted in blue. Theoretical lines of the expected excess noise assuming two channels carrying the current are plotted in dashed lines. The expected excess noise should follow $S_{exc} = 2eI_1(1-t_1) + 2eI_2(1-t_2)$, with $I_1 = \alpha I$ and $I_2 = (1-\alpha)I$ being the currents carried by each channel. Lines are plotted for α=0.5 0.4 0.3 0.2 0.1 and 0.0 (red to

black) where the α=0 case reduces to the single channel scenario. The experimental data, falling on the α=0 line, leads us to conclude a single occupied channel.

Figure S7. **I-V curve of the experiment vs. BCS theory:** (a & b) Measurement of the differential resistance and I-V curves in very low transmission. (c & d) Differential resistance and I-V curves expected from BCS theory assuming a constant transmission in energy.

Figure S8. Each raw show the density of state and the I-V curve for a certain position of the fermi energy (5Δ, 2Δ and Δ above the minimum of the conduction band).

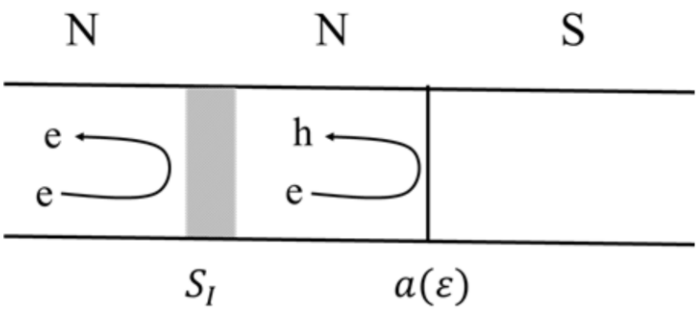

Fig. S1

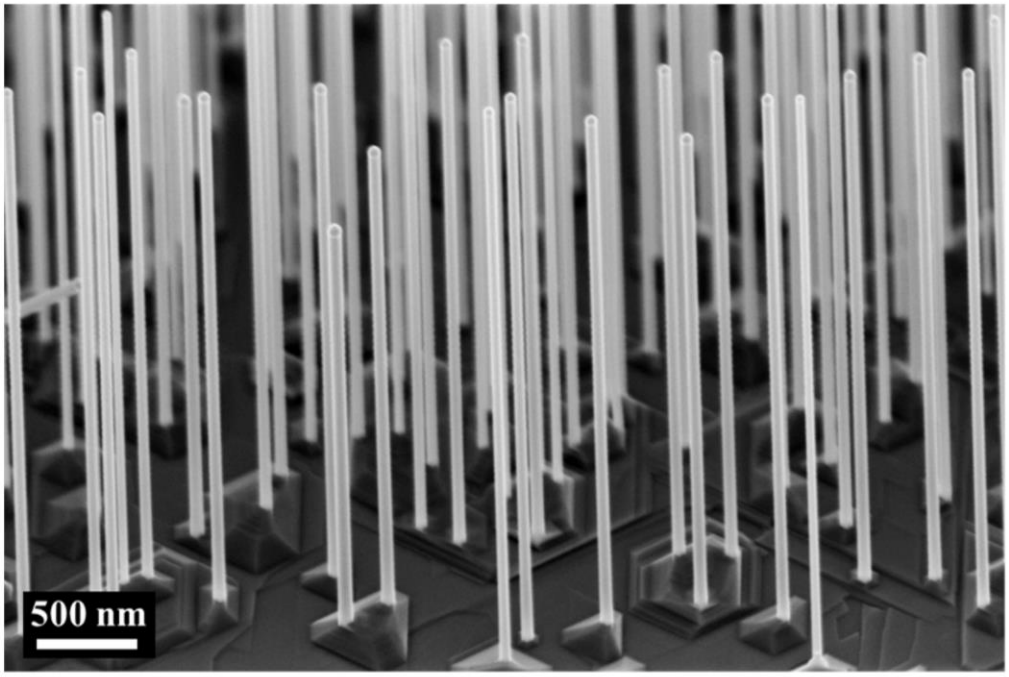

Fig. S2

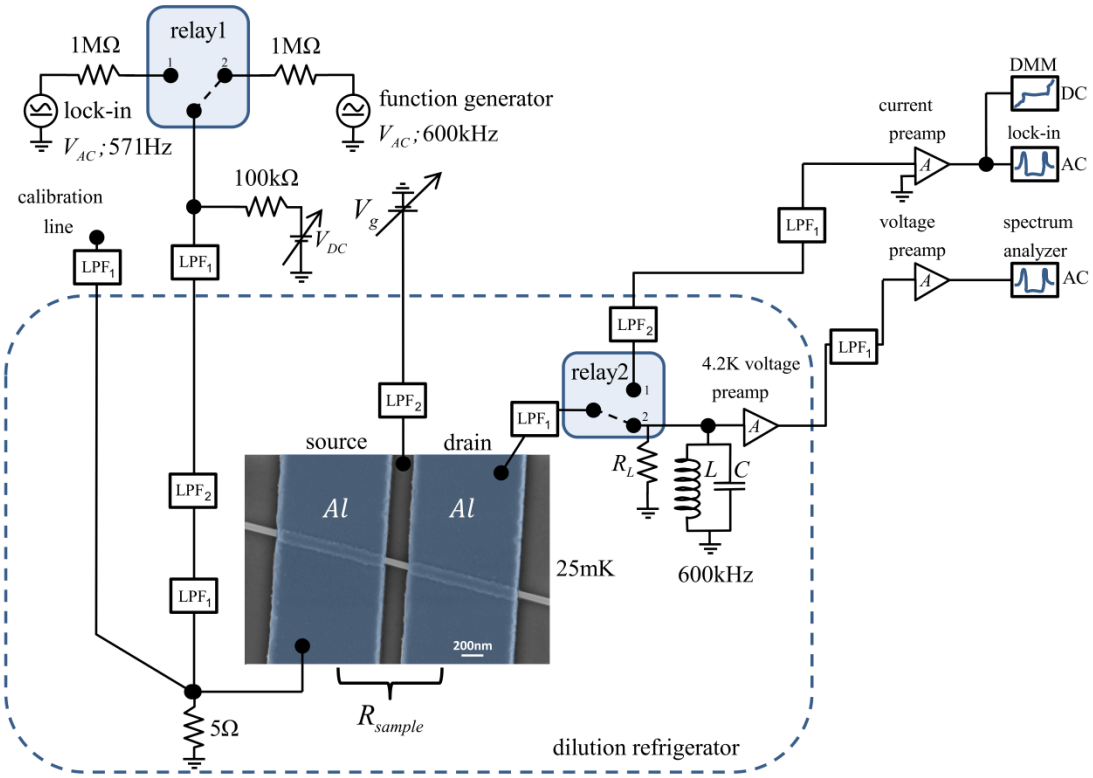
relay1
1MΩ
1MΩ
lock-in
V_{AC};571Hz
function generator
V_{AC};600kHz
100kΩ
V_{DC}
V_g
calibration
line
LPF1
LPF2
source
drain
Al
Al
200nm
25mK
relay2
4.2K voltage
preamp
R_L
L
C
600kHz
current
preamp
DMM
DC
lock-in
AC
voltage
preamp
spectrum
analyzer
AC
5Ω
R_{sample}
dilution refrigerator

Fig. S3

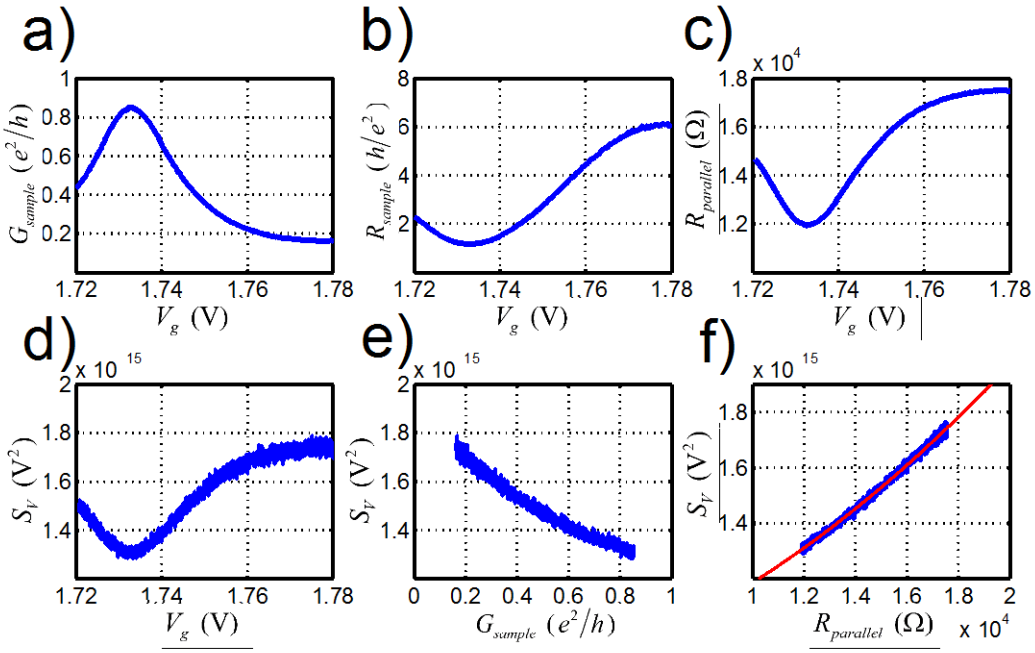
a)
b)
c)
d)
e)
f)
$G_{sample}\ (e^2/h)$
$R_{sample}\ (h/e^2)$
$R_{parallel}\ (\Omega)$
x 10^4
V_g (V)
x 10^15
$S_V\ (V^2)$
$G_{sample}\ (e^2/h)$
$R_{parallel}\ (\Omega)$

Fig. S4

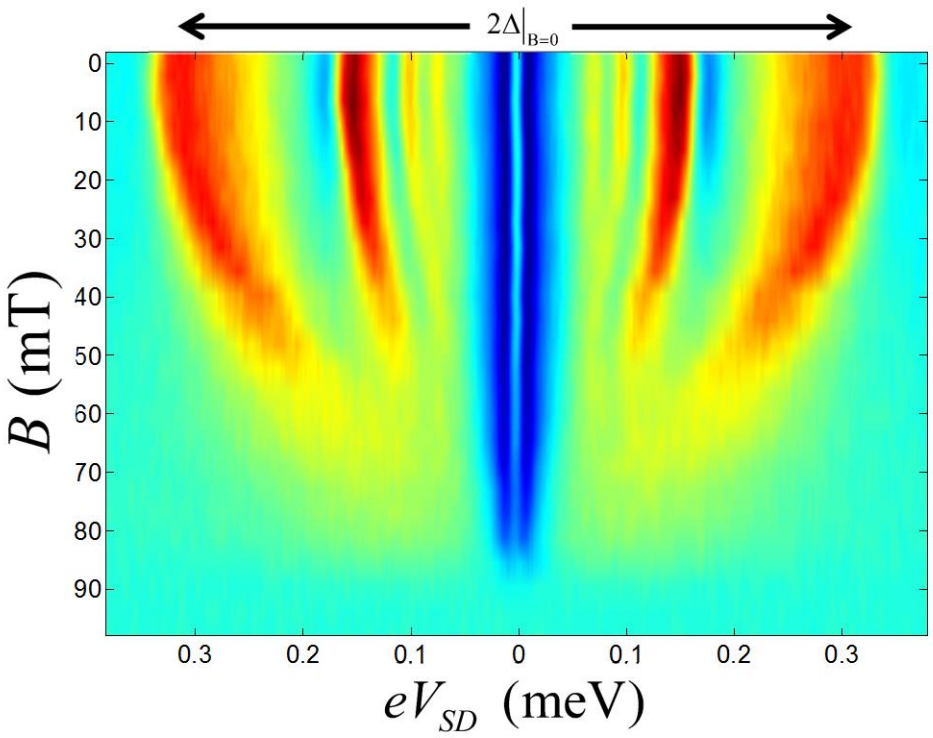
$2\Delta|_{B=0}$
0
10
20
30
40
50
60
70
80
90
B (mT)
0.3
0.2
0.1
0
0.1
0.2
0.3
eV_{SD} (meV)

Fig. S5

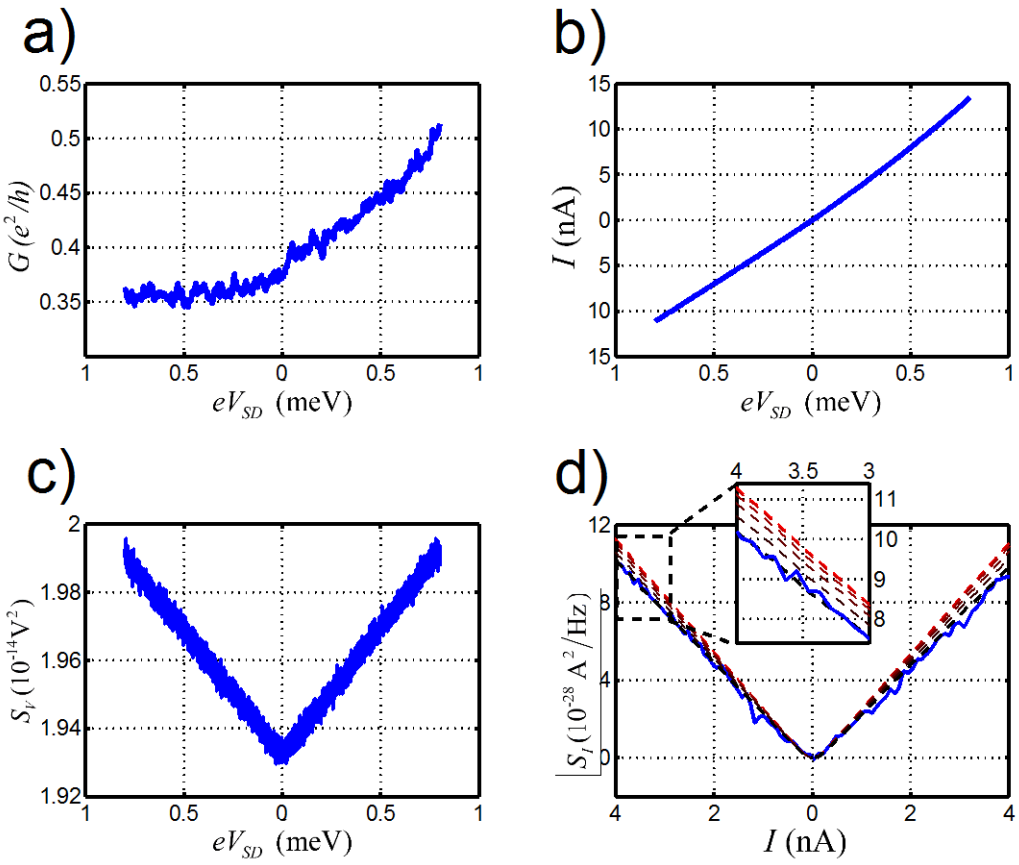
a)
b)
c)
d)
$G\,(e^2/h)$
eV_{SD} (meV)
I (nA)
$S_V\,(10^{-14}\mathrm{V}^2)$
$S_I\,(10^{-28}\,\mathrm{A}^2/\mathrm{Hz})$

Fig. S6

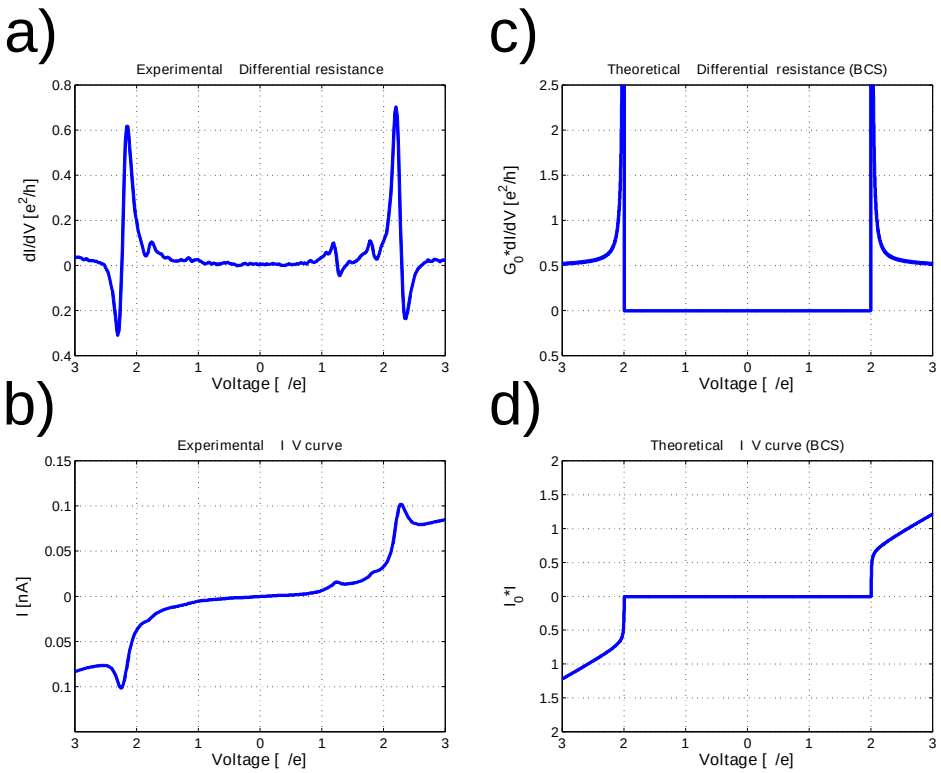
a)
Experimental Differential resistance
dI/dV [e²/h]
Voltage [/e]
c)
Theoretical Differential resistance (BCS)
G₀*dI/dV [e²/h]
Voltage [/e]
b)
Experimental I V curve
I [nA]
Voltage [/e]
d)
Theoretical I V curve (BCS)
I₀*I
Voltage [/e]

Fig. S7

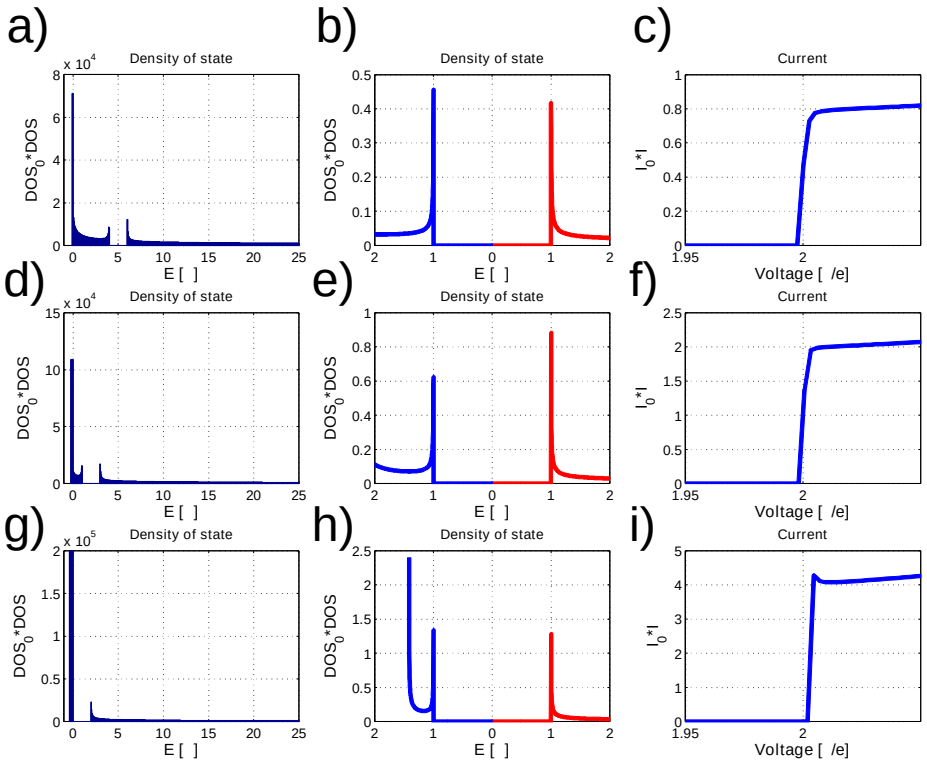
a)
b)
c)
d)
e)
f)
g)
h)
i)
Density of state
Current
DOS0*DOS
I0*I
E [ ]
Voltage [/e]
x 10^4
x 10^5

Fig. S8